# INFLUENCE OF STREAMWISE ROTATION ON PLANE COUETTE FLOW WITH A PASSIVE SCALAR

**Geert Brethouwer**
FLOW, Department of Engineering Mechanics
KTH
Stockholm, SWEDEN
geert@kth.se

## ABSTRACT

We have investigated fully developed turbulent plane Couette flow subject to rotation about the streamwise axis through DNS. In the simulations, we have also included a passive scalar to study the effect of rotation on turbulent scalar transport. We observe a significant secondary mean flow, which is strongest for $Ro \approx 1$. Very large-scale and oblique flow structures also develop. At low rotation rates, the Reynolds analogy between momentum and scalar transport applies, but as the rotation rate increases, scalar transport becomes faster than momentum transport. We also observe that the turbulent Prandtl number becomes less than unity when the flow is subject to streamwise rotation.

## INTRODUCTION

Plane turbulent channel flow subject to streamwise system rotation has been investigated extensively, both experimentally and numerically, see e.g. Oberlack *et al.* (2006); Yang & Wang (2018); Hu *et al.* (2023, 2024) and references therein. A key finding is that streamwise rotation induces a secondary mean flow and leads to the formation of elongated, oblique vortical structures near the walls.

By constrast, the influence of streamwise system rotation on plane Couette flow (PCF) has received much less attention, and also its influence on the heat transfer has hardly been investigated. Recently, the author has studied the stability of PCF and plane Poiseuille flow using linear stability analysis and DNS (Brethouwer, 2025). This study showed that streamwise rotation can strongly reduce the critical Reynolds number of transitions, and that the most unstable modes are highly inclined relative to the streamwise direction when $Ro \approx O(1)$. The critical Reynolds decreases to as low as $Re = U_w\delta/\nu = 20.7$ for streamwise rotating PCF and $Re = U_{cl}\delta/\nu = 66.45$ for streamwise rotating Poiseuille flow in the limit $Ro \to \infty$. Here, $Ro = 2\Omega\delta/U_w$ and $Ro = 2\Omega\delta/U_{cl}$ for PCF and plane channel flow, respectively, with $\Omega$ the rotation rate, $\delta$ the half channel gap-width, and $U_w$ the velocity of the two walls in PCF and $U_{cl}$ the centreline velocity in plane Poiseuille flow. For both $Ro \to 0$ and $Ro \to \infty$ the critical modes increasingly align with the stream direction.

The objective of the present work is to investigate the influence of streamwise system rotation on fully developed turbulent PCF as well as on turbulent heat transfer. Specifically, we examine how system rotation influences the mean flow, Reynolds stresses and turbulent structures, as well as the turbulent heat transport. Owing to its fundamental character, this flow configuration may also serve as a valuable benchmark for turbulence and heat-transfer modelling. Notably, RANS modelling of streamwise-rotating turbulent channel flow has proven challenging (Oberlack *et al.*, 2006).

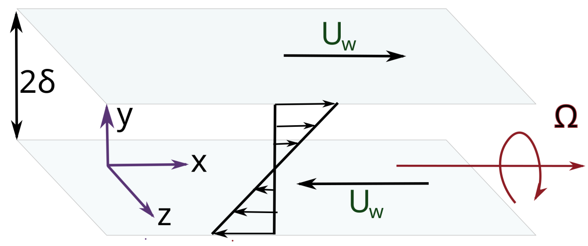


Figure 1. The configuration of streamwise rotating PCF.

## SIMULATION DETAILS

Figure 1 illustrates the flow geometry considered. We perform DNS of incompressible and fully developed turbulent plane Couette flow (PCF) subject to rotation about the streamwise $x$-axis. Two series of DNS have been carried out: one at a fixed Reynolds number $Re = U_w\delta/\nu = 1500$ and one at a fixed $Re = 4000$. The corresponding friction Reynolds number based on the half channel width of the non-rotating reference cases are $Re_\tau = 93$ and 220, respectively, in full agreement with the DNS by Lee & Moser (2018).

In the two DNS series, the rotation number is varied in the ranges $0 \leq Ro \leq 12$ and $0 \leq Ro \leq 2.4$, respectively. These ranges cover the regimes where the critical Reynolds number for transition and the inclination of the most unstable modes relative to the streamwise direction change significantly (Brethouwer, 2025). To examine turbulent heat transfer, a passive scalar with Prandtl number $Pr = 1$ is introduced in all simulations. Isothermal boundary conditions are imposed, with temperatures fixed at $\pm T_w$ at the two walls.

In all DNS, the computational domain size is $60\pi\delta \times 2\delta \times 20\pi\delta$ in the streamwise ($x$-), wall-normal ($y$-), and spanwise ($z$-) directions, respectively. Such large domains are necessary because the flow structures that develop in streamwise rotating PCF can reach very large scales for certain $Ro$, as shown later. The presence of these large structures also leads to long characteristic time scales, meaning that simulations must run for extended periods both to achieve statistically stationary states and to obtain well-converged statistics.

Although the Reynolds numbers considered are relatively modest, the simulations are computationally demanding due to

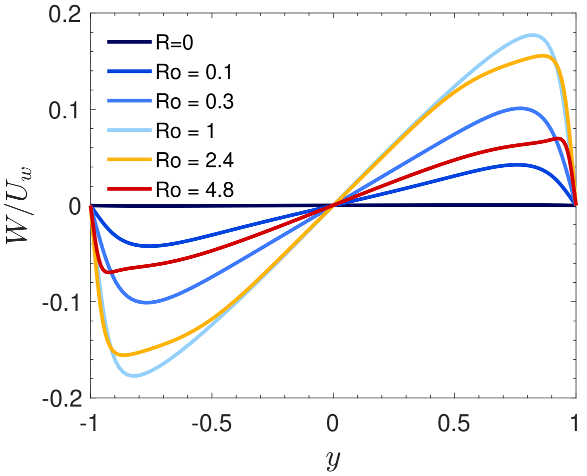


Figure 2. Profiles of the spanwise mean velocity $W$ in the DNS at $Re = 1500$.

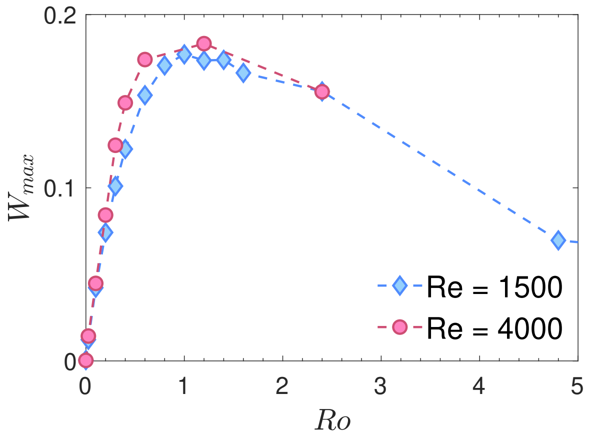


Figure 3. The peak value of $W$ as a function of $Ro$ in the DNS at $Re = 1500$ and $Re = 4000$.

the very large computational domain sizes (requiring up to 1.8 billion grid points at $Re = 4000$ to fully resolve the turbulence) and the long integration times needed.

## DNS RESULTS

Streamwise system rotation has a profound effect on turbulent PCF. All six Reynolds stress components become non-zero, and a secondary mean flow develops. Figure 2 shows the mean spanwise velocity profile $W$ at $Re = 1500$ for $0 \leq Ro \leq 4.8$ and figure 3 shows the maximum $W$ observed in the DNS series at $Re = 1500$ and 4000 as a function of $Ro$. Here $W$ is scaled with $U_w$. At low $Ro$, the $W$-profile is approximately linear in the channel centre. At first, $W$ increases with $Ro$, reaching a maximum of $W/U_w \approx 0.18$ at $Ro = O(1)$, before decreasing. Thus, the secondary mean flow induced by streamwise rotation is substantial, especially for $Ro = O(1)$. This behaviour is similar to that observed in DNS of streamwise rotating channel flow, where the secondary mean flow also peaks at $Ro = O(1)$ (Hu *et al.*, 2023), although with a lower amplitude (the maximum $W \approx 0.1U_{cl}$ at $Re_\tau = 180$).

Figure 4 shows the mean spanwise velocity gradient $(dW/dy)/(U_w/\delta)$ as a function of $Ro$ at the centreline of PCF at $Re = 1500$. In the present DNS, $(dW/dy)/(U_w/\delta) \simeq 0.5Ro$ (shown by the red line in figure 4) at low $Ro$, which means that $dW/dy \simeq \Omega$ and the mean streamwise vorticity is parallel

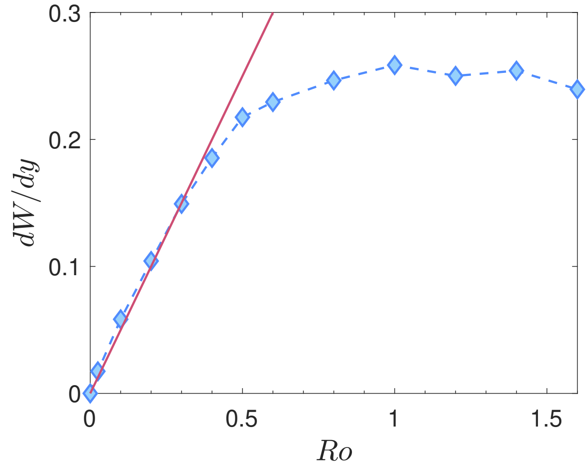


Figure 4. Profiles of the spanwise mean velocity gradient $(dW/dy)/(U_w/\delta)$ at the centreline as a function of $Ro$ in the DNS at $Re = 1500$.

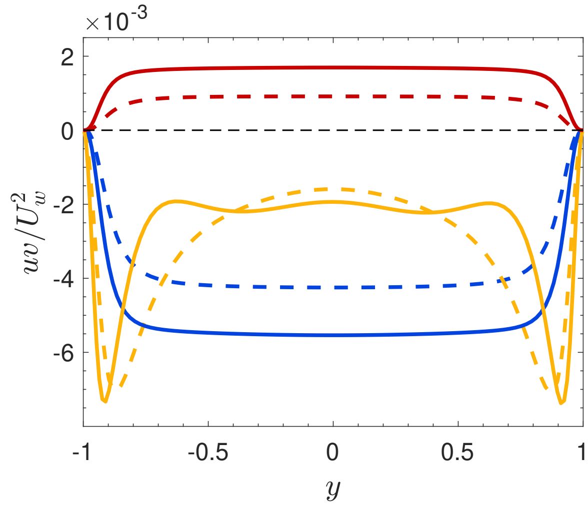


Figure 5. The Reynolds shear stresses $\langle uv \rangle$ (blue lines), $\langle uw \rangle$ (yellow lines) and $\langle vw \rangle$ (red lines) at $Ro = 0.4$ (dashed lines) and $Ro = 1$ (solid lines) in the DNS at $Re = 1500$.

to the system rotation. By contrast, in *spanwise* rotating PCF and channel flow, the mean shear tends toward $dU/dy = 2\Omega$, and the mean spanwise vorticity is anti-parallel to the system rotation (Brethouwer, 2017, 2021).

Figure 5 shows the three Reynolds shear stresses $\langle uv \rangle$, $\langle uw \rangle$ and $\langle vw \rangle$ at $Ro = 0.4$ and $Ro = 1$ and $Re = 1500$. Here, $u$, $v$ and $w$ are the streamwise, wall-normal and spanwise velocity fluctuations. In the DNS, $\langle vw \rangle$ is quite small, but the magnitude of the near-wall peaks of $\langle uw \rangle$ are larger than $\langle uv \rangle$.

Figure 6 shows the mean wall shear stress $\tau_w$ as a function of $Ro$ at $Re = 1500$ and 4000. Here, $\tau_w$ is normalized by $\tau_w$ at $Ro = 0$. The mean wall shear stress, and thus $Re_\tau$, increases monotonically with $Ro$ in the $Re = 1500$ series, while at $Re = 4000$ it first decreases slightly before increasing steadily. The wall-normal and spanwise velocity fluctuations also increase almost monotonically with $Ro$ in the DNS at $Re = 4000$ (not shown). In particular, the root-mean-square of the wall-normal fluctuations grows in the channel centre, while that of the spanwise fluctuations nearly doubles near the walls.

Visualizations of the instantaneous streamwise velocity in

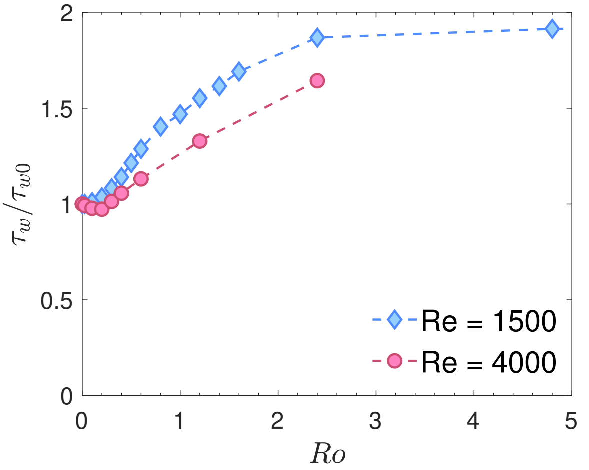


Figure 6. Normalized mean wall shear stress in the DNS at $Re = 1500$.

the midplane at $Re = 1500$, shown in figure 7, illustrate the impact of streamwise rotation on the turbulent structures. At $Ro = 0$, large-scale streamwise-aligned structures with a spanwise wavelength of about $5\delta$ are visible, consistent with the DNS results of Lee & Moser (2018). With increasing $Ro$, the structures become clearly inclined relative to the streamwise direction and grow significantly in size, as seen in the visualization at $Ro = 0.8$ and $Ro = 1.4$. Large velocity jumps are also observed in the visualization. In addition, the Reynolds shear stresses are concentrated in coherent oblique bands, as shown in figure 8. However, with increasing $Ro$ both the inclination and the size of the structures decrease, as seen in the visualization at $Ro = 2.4$. Similar trends are observed in the DNS series at $Re = 4000$.

These observations are consistent with linear stability analysis, which predicts that the critical modes are most inclined at $Ro = O(1)$ and align with the streamwise direction in the limits $Ro \to 0$ and $Ro \to \infty$. In streamwise rotating channel flow, near-wall vortical structures show analogous behaviour (Hu *et al.*, 2023). That is, the vortical structures are most inclined to the streamwise direction for $Ro = O(1)$, although their inclination remains below $10^\circ$, i.e. less than in PCF. Furthermore, the spanwise wavelength of the structures in streamwise rotating PCF grows to about $20\delta$ at $Ro = 0.8$ according to the visualization in figure 7, several times larger than in non-rotating PCF, whereas in streamwise rotating channel flow the spanwise scale remains much smaller and nearly constant at about $2.4\delta$ (Yang & Wang, 2018).

Streamwise rotation also strongly affects turbulent passive scalar transport. Figure 9 shows the mean temperature profiles at $Re = 1500$, which become increasingly flat in the centre region when $Ro$ increases. The mean temperature gradient becomes even slightly negative at the centreline at $Ro = 2.4$, which means that the turbulent scalar transport becomes counter gradient. Figure 10 shows the Nusselt number $Nu = (dT/dy)_w/(T_w/\delta)$ for scalar transport in the DNS at $Re = 1500$ and 4000. Here, $(dT/dy)_w$ is the mean temperature gradient at the wall. In the figure, $Nu$ is normalized by the Nusselt number at $Ro = 0$, $Nu_0$. Like $\tau_w$, $Nu$ increases monotonically with $Ro$ at $Re = 1500$, whereas it first slightly decreases and then monotonically increases with $Ro$ at $Re = 4000$. This shows that streamwise rotation can significantly increase the momentum and scalar transport. Figure 11 shows the Reynolds analogy factor RA, which is defined as the ratio of $(dT/dy)_w/(T_w/\delta)$ to $(dU/dy)_w/(U_w/\delta)$

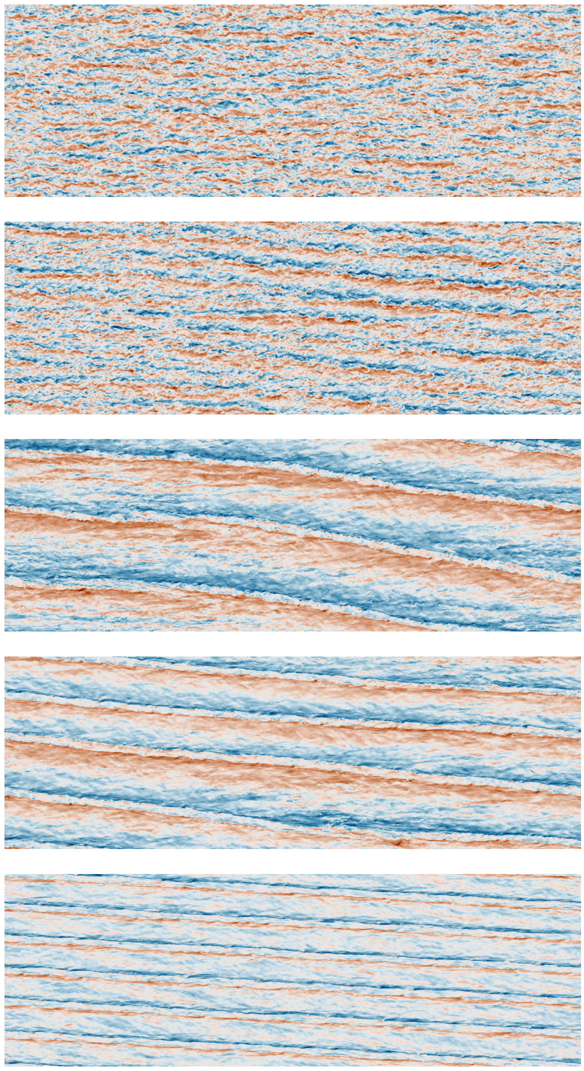

Figure 7. Visualizations of the instantaneous streamwise velocity in the midplane of the DNS at $Re = 1500$ and (from top to bottom) $Ro = 0$, $Ro = 0.1$, $Ro = 0.8$, $Ro = 1.4$ and $Ro = 2.4$.

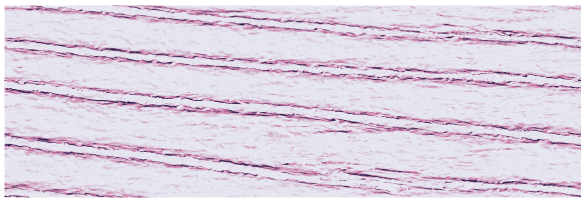

Figure 8. Visualizations of the instantaneous Reynolds shear stress $uv$ in the midplane of the DNS at $Re = 1500$ and $Ro = 1.4$.

in the DNS. Here, $(dT/dy)_w$ and $(dU/dy)_w$ are the mean temperature and mean streamwise velocity gradients at the wall, respectively. RA is the ratio of scalar transport to momentum transport, which is unity when the Reynolds analogy applies. In the present DNS, RA is unity at $Ro = 0$ but increases with $Ro$ to approximately 1.3 at $Re = 1500$ and 1.2 at $Re = 4000$, showing that in streamwise rotating PCF, scalar transport becomes more efficient than momentum transport.

Figure 12 shows the turbulent Prandtl number $Pr_T$ in the DNS at $Re = 1500$. In non-rotating PCF, the Reynolds analogy between momentum and scalar transport holds with a tur-

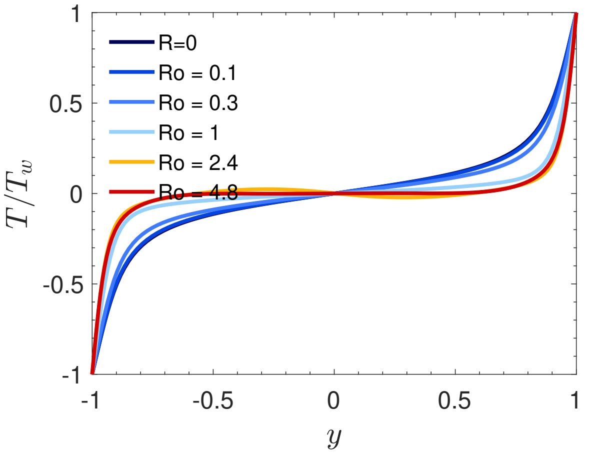


Figure 9. Mean temperature profiles in the DNS at $Re = 1500$.

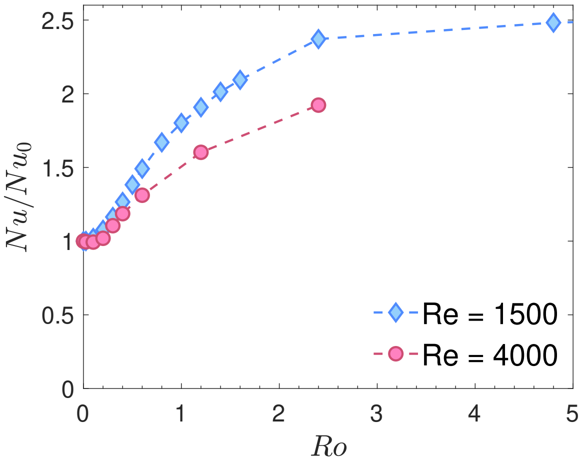


Figure 10. Normalized Nusselt number as a function of $Ro$ in the DNS at $Re = 1500$ and $Re = 4000$.

bulent Prandtl number $Pr_T \approx 1$ across the channel, consistent with results for other non-rotating turbulent shear flows. Under the influence of streamwise rotation, however, scalar transport exceeds momentum transport, as we have shown, breaking the Reynolds analogy. Accordingly, as shown in figure 12, $Pr_T$ decreases with increasing $Ro$, indicating a larger eddy diffusivity for the scalar than the eddy viscosity. At $Ro = 2.4$, $Pr_T$ even becomes negative near the channel centre, consistent with the observed counter-gradient transport.

In the presentation, we will provide additional results on turbulence statistics and energy spectra to further characterize the large-scale structures, as well as a more detailed analysis of scalar transport in streamwise rotating PCF.

## REFERENCES

Brethouwer, G. 2017 Statistics and structure of spanwise rotating turbulent channel flow at moderate Reynolds numbers. *J. Fluid Mech.* **828**, 424–458.

Brethouwer, G. 2021 Much faster heat/mass than momentum transport in rotating Couette flows. *J. Fluid Mech.* **912**, A31.

Brethouwer, G. 2025 Stability of plane Couette and Poiseuille flows rotating about the streamwise axis. *J. Fluid Mech.* **1021**, A14.

Hu, R., Li, X. & Yu, C. 2023 Multiscale dynamics in streamwise-rotating channel turbulence. *J. Fluid Mech.* **972**, A14.

Hu, R., Li, X. & Yu, C. 2024 Effects of streamwise rotation on helicity and vortex in channel turbulence. *J. Fluid Mech.* **980**, A50.

Lee, M. & Moser, R. D. 2018 Extreme-scale motions in turbulent plane Couette flows. *J. Fluid Mech.* **842**, 128–145.

Oberlack, M., Cabot, W., Reif, B. A. Pettersson & Weller, T. 2006 Group analysis, direct numerical simulation and modelling of a turbulent channel flow with streamwise rotation. *J. Fluid Mech.* **562**, 383–403.

Yang, Z. & Wang, B.-C. 2018 Capturing Taylor-Görtler vortices in a streamwise-rotating channel at very high rotation numbers. *J. Fluid Mech.* **838**, 658–689.

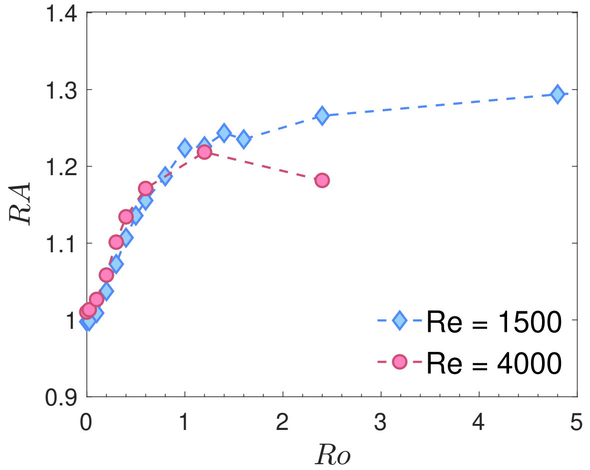


Figure 11. Reynolds analogy factor RA as a function of $Ro$ in the DNS at $Re = 1500$ and $Re = 4000$.

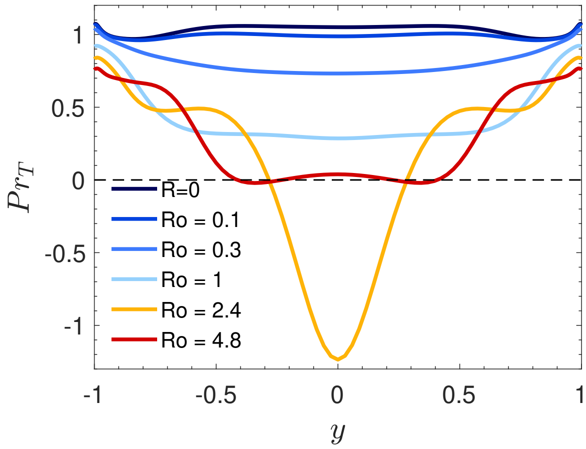


Figure 12. Turbulent Prandtl number $Pr_T$ in the DNS at $Re = 1500$.